Behavioral/Systems/Cognitive

In Vivo Intracellular Recording Suggests That Gray Matter Astrocytes in Mature Cerebral Cortex and Hippocampus Are Electrophysiologically Homogeneous

Tsuneko Mishima[1] **and Hajime Hirase**[1,2]

[1]Hirase Research Unit, RIKEN Brain Science Institute, Wako, Japan, and [2]Saitama University Brain Science Institute, Saitama 338-8570, Japan

Previous anatomical and *in vitro* electrophysiology studies suggest that astrocytes are heterogeneous in physiology, morphology, and biochemical content. However, the extent to which this diversity applies to *in vivo* conditions is largely unknown. To characterize and classify the physiological and morphological properties of cerebral cortical and hippocampal astrocytes in the intact brain, we performed *in vivo* intracellular recordings from single astrocytes using anesthetized mature rats. Astrocytes were classified based on their glial fibrillary acidic protein (GFAP) immunoreactivity and cell body locations. We analyzed morphometric measures such as the occupied volume and polarity, as well as physiological characteristics such as the mean membrane potential. These measurements did not show obvious segregation into subpopulations, suggesting that gray matter astrocytes in the cortex and hippocampus are composed of a homogeneous population in mature animals. The membrane potential of astrocytes in both cortex and hippocampus fluctuated within a few millivolts in the presence of spontaneous network activity. These membrane potential fluctuations of an astrocyte showed a significant variability that depended on the local field potential state and cell body location. We attribute the variability of the membrane potential fluctuations to local potassium concentration changes due to neuronal activity.

Introduction

Astrocytes support the normal operation of neuronal circuitry, regulating the extracellular potassium concentration and the clearance of synaptically released glutamate. In rodent cerebral cortex, astrocytes occupy 20–30% of the cell population (Nedergaard et al., 2003). Astrocytes have traditionally been described as forming a relatively homogeneous population characterized by a highly negative resting membrane potential, low input resistance, and extensive intercellular coupling via gap junctions (Kuffler et al., 1966; Picker et al., 1981; Casullo and Krnjevic, 1987). In the last decade, heterogeneity of astrocyte population has became a matter of controversy (Walz, 2000). For instance, astrocytes devoid of glial fibrillary acidic protein (GFAP) expression have been reported (Walz and Lang, 1998). Moreover, astrocytes that have voltage-dependent active conductance have been described (Zhou and Kimelberg, 2000, 2001; Seigneur et al., 2006) and the proportion of active-conductance astrocytes was shown to vary during the course of development (Zhou et al., 2006). Transgenic mice expressing green fluorescent protein (GFP) under a GFAP promoter label a subset of astrocytes in the hippocampus (Nolte et al., 2001). Glutamate transporter currents are recorded from cells with a high level of GFP expression (GluT cells), and functional AMPA receptors are expressed in cells with weaker levels of GFP (GluR cells) (Matthias et al., 2003), suggesting that these GluR cells are likely to be oligodendrocyte precursor cells (Bakiri et al., 2009). Recently, astrocytes within a column of the barrel cortex have been shown to connect preferentially with gap junctions (Wallraff et al., 2006; Houades et al., 2008), and evoked calcium activity shows a similar clustering within barrel columns (Wang et al., 2006; Schipke et al., 2008).

Despite these findings, whether there is a functional diversity in astrocytes has hardly been studied *in vivo*, partly because of technical difficulties in intracellular recording and labeling of single astrocytes. We recently reported that the use of biotinylated dextran amine 10 kDa (BDA-10000) is a practical solution to label intracellularly recorded glial cells *in vivo* (Mishima et al., 2007). In the current study, we used this method to perform *in vivo* intracellular recordings from astrocytes in the rat cerebral cortex and hippocampus, and assessed whether astrocytes can be classified into different subpopulations.

Materials and Methods

Surgery and electrophysiological recording. In vivo intracellular recordings were performed as described in detail in Mishima et al. (2007). Briefly, 218 male Sprague Dawley rats weighing 150–300 g (4–6 weeks postnatal) were anesthetized with urethane (1.7 g/kg). The body temperature of rats was kept at 37°C by a heat pad placed underneath the animal. Under these conditions, cortical EEG states spontaneously alternate between synchronized and desynchronized states (e.g., Wolansky et al., 2006; Takata and Hirase, 2008). After the animal was rigidly fixed in a stereo-

Received Oct. 10, 2009; revised Jan. 13, 2010; accepted Jan. 18, 2010.

This work was supported by a Grant-in-Aid for Scientific Research on Priority Areas from the Ministry of Education, Culture, Sports, Science, and Technology of Japan (Grant 18053026) and RIKEN Brain Science Institute intramural research funds. H.H. was supported by the Human Frontier Science Program (RGY0073/2006). We thank Kazuko Yahagi, Iori Tomizawa, and RIKEN BSI-Olympus Collaboration Center for technical support. We thank Yoshiaki Shinohara for supplying molecular tools to visualize astrocytic morphology. We are grateful to Takeshi Kanda, Norio Takata, Kentaroh Takagaki, Attila Sik, Philip G. Haydon, and anonymous referees for advice and fruitful discussion.

Correspondence should be addressed to either Tsuneko Mishima or Hajime Hirase, Hirase Research Unit, RIKEN Brain Science Institute, Wako-shi 351-0198, Japan. E-mail: mishima@brain.riken.jp or hirase@brain.riken.jp.

DOI:10.1523/JNEUROSCI.5065-09.2010

 0270-6474/10/303093-08$15.00/0

taxic apparatus, the scalp was removed and a small craniotomy (diameter ~1.5 mm) was made at stereotaxic coordinates of anterior–posterior −4.0 mm and lateral 2.2 mm from bregma, which corresponds to the somatosensory cortex. Once durotomy was completed, the craniotomy was filled with physiological saline to prevent the brain surface from drying. The intracellular electrode was made from a thick wall borosilicate glass pipette (1B150F-4, World Precision Instruments). The tip of the electrode was back-filled with pH-adjusted (pH range: 7.2–8.0) 1.0 M potassium acetate solution containing 4% BDA-10000 (D1956, Invitrogen). The electrode was then gently filled with 1.0 M potassium acetate. The resistances of electrodes ranged from 50 to 150 MΩ. The intracellular electrodes were attached to a remotely driven micromanipulator (PC-5N, Narishige, modified for custom use). Intracellular recording was made with a programmable DC bridge amplifier (Multiclamp 700B, Molecular Devices). The electrode was advanced with a 1–2 μm step using the fastest acceleration mode. A high-frequency buzz of 10 ms was exerted through the headstage preamplifier to establish intracellular penetration. After intracellular penetration, we readjusted the electrode resistance using the short pulse bridge balance method (Sugimori et al., 1978). Briefly, a 0.5 nA, 1 ms positive current pulse was generated and the electrode capacitance was neutralized. To compensate the series resistance, the peak potential of the charging voltage was adjusted to baseline with the bridge balance. Using this method, the electrode capacitance was compensated and the bridge was kept balanced before measurement of input resistance and membrane potential. Brief hyperpolarizing current pulses (−500 to −50 pA, 250 ms) were injected to determine the input resistance of the cell. After electrophysiological measurements were completed, a depolarizing current was injected repeatedly (500–1000 pA, 120–250 ms, 1–3 Hz) through the intracellular electrode for 10–50 min to fill the cell with BDA-10000.

To monitor neuronal activity, a 16 channel silicon probe (NeuroNexus Technologies) was inserted in the cerebral cortex or hippocampus. Signals from these electrodes were buffered (TLC2274AC, Texas Instruments, or HS-27 preamplifier module, Neuralynx), filtered (1–9000 Hz), and amplified (×2000 gain, L8 Amplifier, Neuralynx) before digitization. All electrophysiological signals were digitized with 16-bit resolution at 25 kHz sampling rate and stored on a hard drive using custom software written with LabVIEW (National Instruments).

All experimental protocols were approved by the RIKEN Institutional Animal Care and Use Committee.

Histology. Thirty to sixty minutes after the filling procedure, animals were transcardially perfused with 100 ml of physiological saline (0.9% NaCl), followed by 200 ml of 4% paraformaldehyde in 0.1 M phosphate buffer (PB). The recorded area was dissected and postfixed for 10–24 h at 4°C. Coronal sections were cut at 60 μm thickness in 0.1 M PB, pH 7.4, using a vibratome (Pro-7 Linear Slicer, DSK). Cell morphology was visualized by a combination of avidin–biotin complex and tyramide signal amplification techniques (Mishima et al., 2007). Immunohistochemistry was performed in 0.1 M PB or 0.05 M Tris-buffered saline (TBS) containing rabbit anti-GFAP (1:1000, G-3893, Sigma) or rabbit anti-S100B antibody (1:2000, 611516, JIMRO, or 37, Swant) and 0.1–0.3% Triton X-100 for a minimum of 12 h. In some experiments anti-NG2 antibody (1:400, AB5320 Millipore Bioscience Research Reagents or 1:200, 05-710, Millipore) was also used. After rinsing three times in PB or TBS, sections were incubated with fluorophore-conjugated secondary antibodies (CY3, 1:1000, Jackson ImmunoResearch; or Alexa Fluor, 1:1000 Invitrogen) and then mounted with an anti-fading medium (Vectashield H-1200, Vector Laboratories). Labeled sections were imaged with confocal microscopes (FV-500 or FV-1000, Olympus). Once the fluorescent images were captured, sections were further developed with a standard diaminobenzidine nickel (DAB-Ni) peroxidase method for long-term storage.

Analysis. The position of a recorded cell was quantified by distance from the brain surface. To compute the occupied volume of a single astrocyte, the three-dimensional (3D) confocal image stacks were smoothed by applying pixelwise dilation processing for three to five times, followed by application of erosion processing for the same number of times. 3D image stacks were then treated with a hole-filling algorithm for each 2D image in the stack. The resultant 3D stack image contained a smoothed silhouette of the astrocyte with all internal pixels filled, from which the occupied volume was estimated. To calculate the polarity index, an ellipsoid encompassing the whole astrocyte was fitted using a Matlab (MathWorks) program. The polarity index is defined as the ratio of the longest axis and the shortest axis of the semiprincipal axes.

The input resistance (R_{in}) was calculated as the slope of an *I–V* curve, as defined by the voltage deflections in response to a brief current injection to the cell. The voltage deflection was calculated as the mean of the plateau potential.

Spontaneously occurring local field potential (LFP) events and membrane potentials of single astrocytes were analyzed by custom-made software using Matlab on a Linux-based computer. The mean membrane potential was defined as the average membrane potential trace over a stably recorded period. The membrane potential fluctuation was defined as the mean of the SDs of 1 s membrane potential trace segments.

Astrocytic membrane potential traces were averaged based on LFP event triggers, which were detected as described by Sakatani et al. (2007). Briefly, the raw wide-band extracellular recording data were first downsampled to 1.25 kHz. For cortical LFP, the resampled signal from layer 5 was bandpass filtered (300–500 Hz) to emphasize the high-frequency activity (i.e., multiunit activity). The filtered signal was squared and convolved with a Hanning window of 100 ms to smooth the outcome. A threshold was applied to detect the onset of UP states. Similarly, characteristic hippocampal LFP patterns, such as theta and ripple oscillations, were automatically detected by thresholding the smoothed root-mean-square power of the respective (3–8 Hz and 100–180 Hz) frequencies. To detect CA1 ripple events, the root-mean-square power of the LFP signal taken from stratum pyramidale was computed and smoothed with a Hamming window of 20 ms. CA1 ripple events were detected by applying an amplitude threshold (mean + 10 SD) to the smoothed root-mean-square power data. The maximum negative voltage of LFP was defined as the center of a ripple event, and used as the trigger points.

Distribution of measured and calculated values are plotted as box plots, where the whiskers represent the bottom 10th and 90th percentiles, the boundaries represent the bottom 25th and 75th percentiles. The horizontal line in the middle of each box represents the median. Values are expressed as mean ± SD, unless otherwise noted.

Results

Database and cellular identification by histological visualization

Recordings were considered to be from glial cells when they satisfied all of the following criteria: (1) The impalement was accompanied by a sudden drop of the membrane potential to −40 mV or below; (2) No spontaneous action potentials were observed during or after the impalement; (3) Action potentials could not be evoked in response to depolarizing current injection (100–500 pA). One hundred of these glial cells were identified histologically, out of attempts made in 218 animals. Putative glial cells that could not be histologically recovered were not included in subsequent analyses. Astrocytes were identified histologically by their characteristic appearance, with radially spreading processes ramifying into numerous microprocesses. Out of the 100 cells in the database, 54 cells were located in the cerebral cortex (layer I–VI), four cells were located in the white matter, and 42 cells were located in the hippocampus. Ninety-two cells had an astrocytic morphology (92%), 6 cells had an oligodendrocytic morphology (6%), and 2 cells had a microglia-like morphology (2%).

Gross morphological properties of astrocytes

Among the cells with astrocytic morphology, 63 cells exhibited strong GFAP immunoreactivity [GFAP(+) cells], and 23 cells had undetectable levels of GFAP immunoreactivity [GFAP(−) cells] (Fig. 1). The remaining 6 putative astrocytes were not tested for GFAP immunoreactivity. As GFAP(−) glia may potentially be NG2 glia, which also have a stellate morphology (Nishiyama et al., 2005), we examined immunoreactivity for the proteoglycan NG2 in addition to GFAP (supplemental Fig. 1, available at

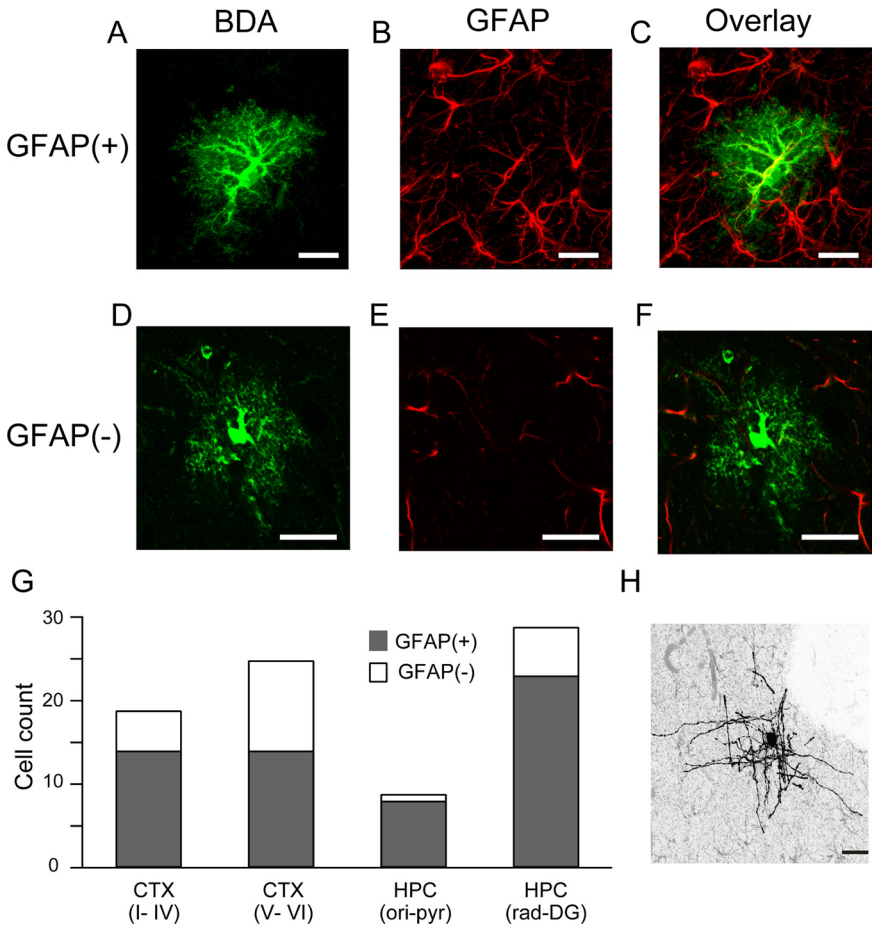

Figure 1. Morphological reconstruction of *in vivo* labeled cortical astrocytes. Confocal images of two astrocytes labeled with BDA-10000 by *in vivo* intracellular injection (***A***, ***D***; green) and immunohistochemistry against GFAP (***B***, ***E***; red) are displayed. Overlay of the images (***C***, ***F***) distinguishes the GFAP(+) astrocyte from the GFAP(−) astrocyte. ***G***, Bar graph shows the total numbers of intracellularly recorded GFAP(+) (gray) and GFAP(−) (white) astrocytes and their locations used in this study. Astrocytes are clearly distinguished from other glial cell types by their morphology, as exemplified by the morphology of an intracellularly filled presumed oligodendrocyte (***H***). Scale bars are 20 μm. CTX, Cortex; HPC, hippocampus; ori, stratum oriens; pyr, stratum pyramidale; rad, stratum radiatum; DG, dentate gyrus.

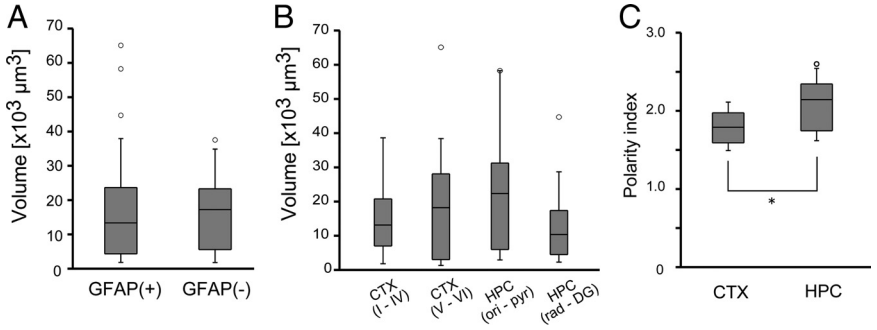

Figure 2. Occupied area and morphological polarity of astrocytes. ***A***, The occupied volume of GFAP(+) and GFAP(−) astrocytes were similar. ***B***, The occupied volume did not depend on the cell body location. ***C***, Astrocyte morphology was more polarized in hippocampus than cortex (*$p < 0.05$, *t* test).

www.jneurosci.org as supplemental material). None of the intracellularly labeled cells showed NG2 immunoreactivity; thus, both GFAP(+) and GFAP(−) cells are all henceforth considered to be astrocytes. GFAP(+) astrocytes occupied 67% and 82% of the astrocytes in the cortex and hippocampus, respectively.

We asked next whether the difference in GFAP expression level is related to the gross morphology of astrocytes. Both GFAP(+) and GFAP(−) cells generally had a spherical soma with primary processes branching into many fine processes (Fig. 1; supplemental Fig. 1, available at www.jneurosci.org as supplemental material). The occupied volume of the GFAP(+) and GFAP(−) astrocytes were $16.4 \pm 14.6 \times 10^3$ μm^3 ($n = 57$) and $16.6 \pm 11.0 \times 10^3$ μm^3 ($n = 15$), respectively. The occupied volume did not differ significantly between GFAP(+) and GFAP(−) astrocytes (Fig. 2*A*) ($p = 0.96$, *t* test). To see how astrocytic territory deviates from a sphere, the polarity index was computed for those astrocytes that had complete morphology within a histological section. The polarity index was also similar in GFAP(+) and GFAP(−) astrocytes (1.9 ± 0.3; $n = 18$ vs 2.0 ± 0.3; $n = 8$; $p = 0.84$, *t* test).

We questioned whether the occupied volume of an astrocyte depends on the cell body location. ANOVA computed no significant difference in the occupied volume in the cerebral cortex (Fig. 2*B*) ($p = 0.45$, Kruskal–Wallis test). The polarity index was larger for hippocampal astrocytes (2.1 ± 0.3, $n = 12$) than cortical astrocytes (1.8 ± 0.2, $n = 13$), suggesting that hippocampal astrocytes occupy more nonspherical (ellipsoidal) volume (Fig. 2*C*) ($p < 0.05$).

Physiological properties of astrocytes

Astrocyte membrane potential was stably recorded and showed modest and slow fluctuations without large changes in the mean membrane potential (Fig. 3*A*). We examined whether the mean membrane potential and membrane potential fluctuations depend on the cell body location or the level of GFAP expression. Overall, the mean membrane potential of individual astrocytes had a Gaussian-like distribution (-86.5 ± 5.4 mV) (Fig. 3). The mean membrane potential was not different between GFAP(+) and GFAP(−) astrocytes (-86.9 ± 5.7 mV vs -86.3 ± 5.0 mV, *t* test, $p = 0.63$) (Fig. 3*E*).

To investigate regional differences in membrane potential, we divided the recorded cells into four groups according to the depth of the soma from the brain surface. Cerebral cortical astrocytes were grouped into two populations separated at a pial depth of 850 μm, which roughly corresponded to the layer IV/V border (group I: layer I–IV; group II: V–VI). Hippocampal astrocytes were grouped into a population whose locations were above the stratum radiatum (stratum oriens and stratum pyramidale: group III) or were in or below the stratum radiatum (group IV). Statistical analysis by ANOVA indicated that the mean membrane potential of astrocytes differ by the region ($p = 0.018$, one-way ANOVA) (Fig. 3*D*). *Post hoc* Tukey–Kramer tests showed that astrocytes in group III (-90.0 ± 4.91 mV,

$n = 9$) had more hyperpolarized mean membrane potential than group II (-85.0 ± 4.91 mV, $n = 28$). Statistical comparisons of all other combinations of populations were not significant.

As previous *in vitro* studies suggest a correlation between GFAP levels, dye-coupling, and AMPA receptor expression (Seifert and Steinhauser, 1995; Wallraff et al., 2004), we investigated the relationship between measured input resistance and GFAP expression (supplemental Fig. 2, available at www.jneurosci.org as supplemental material). The mean input resistance of GFAP(+) astrocytes was 49.0 ± 64.7 ($n = 42$) MΩ, whereas that of GFAP(−) astrocytes was 38.1 ± 45.2 MΩ ($n = 11$). We found no statistically significant difference between the input resistance values of GFAP(+) astrocytes and of GFAP(−) astrocytes ($p = 0.66$, t test). We also examined possible correlation between cell body location and input resistance. The mean input resistances of cortical and hippocampal astrocytes were 57.0 ± 74.8 MΩ ($n = 27$) and 36.80 ± 43.0 MΩ ($n = 27$), respectively. The Kruskal–Wallis test shows no location dependency of astrocyte input resistance ($p = 0.51$). It is reminded as a caveat that the measurements of input resistance based on current injection from a sharp electrode has limited electrical access to the cell and measurements made by whole-cell patch clamp often yields lower and less variable values.

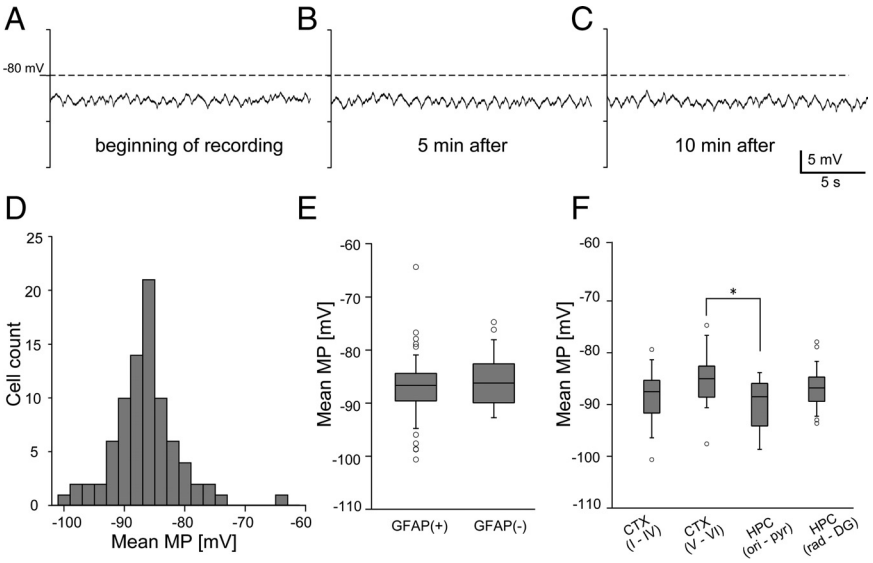

Figure 3. Membrane potential (MP) recording from single astrocytes. Stable membrane potential recording is achieved from a single astrocyte. ***A–C***, Representative trace of single astrocyte membrane potential fluctuations recorded shortly after intracellular penetration (***A***), after 5 min (***B***), and after 10 min (***C***). ***D***, Distribution of the mean membrane potential of all recorded astrocytes shows a mode at around −86 mV. ***E***, Distributions of the mean membrane potential of GFAP(+) and GFAP(−) astrocytes are represented in box plots. GFAP(+) and GFAP(−) cells did not differ significantly in the mean membrane potential. ***F***, Mean membrane potential of astrocytes in different brain regions are represented in box plots (*$p < 0.05$, one-way ANOVA).

EEG state-dependent astrocyte membrane potential

Next, we investigated how the membrane potential of astrocytes changes with surrounding neuronal activity. During the synchronized state, the cortical LFP showed slow oscillations consisting of UP and DOWN states that alternated at 0.5–2 Hz. The membrane potential of cortical astrocytes showed slow oscillations that were coherent with the transitions of UP and DOWN states (U/D) (Fig. 4*A*). The magnitude of astrocytic membrane potential fluctuations in the cerebral cortex during U/D states was 0.65 ± 0.23 mV ($n = 36$) (Fig. 4*C*). The magnitude of the membrane potential fluctuations was significantly smaller during the desynchronized (DS) state (Fig. 4*B*,*C*) (0.38 ± 0.28 mV, $n = 24$, $p < 0.0005$, t test). Next, we compared the astrocytic membrane potential fluctuations between superficial and deep layers in the cortex (Fig. 4*D*). Astrocytic membrane potential fluctuated significantly more in superficial layers of the cortex during the U/D state (0.77 ± 0.18 vs 0.60 ± 0.27 mV, $p < 0.05$, t test), but not during the DS state (0.33 ± 0.11 vs 0.38 ± 0.34 mV, $p = 0.6$, t test). The amplitude of membrane potential fluctuations during the U/D state was not distinguished by GFAP expression level (data not shown; $p = 0.1$, t test). Although the astrocytic membrane potential fluctuation significantly differed between the different LFP states, the mean membrane potential of these astrocytes were similar in both states (Fig. 4*E*) ($p = 0.7$, t test). We compared the membrane potential in hyperpolarized epochs by taking the bottom tenth percentile membrane potential in the two states. On average, the hyperpolarized membrane potential was 1.65 mV more hyperpolarized during the U/D states ($p < 0.05$, paired t test). Thus, the astrocytic membrane potential is tonically depolarized during the DS state.

To investigate the temporal relationship between neuronal activity and astrocytic membrane potential fluctuations, we calculated trigger-averaged astrocytic membrane potential traces by onsets and offsets of UP states. Triggered averaging of cortical LFP (Fig. 5, upper panels) showed that the activity in the superficial layer precedes activity in the deep layer for both onsets and offsets of UP states. In agreement with previous studies (Amzica and Steriade, 2000; Amzica and Massimini, 2002; Amzica et al., 2002), astrocytic membrane potential depolarized with UP states (Fig. 5, lower panels). Moreover, the depolarization onset was earlier in superficially located cortical astrocytes (<1000 μm depth from the pial surface) than in deeply located cortical astrocytes. Population data showed that the depolarization onset for deeply located astrocytes was delayed by ~30 ms from that of more shallowly located astrocytes. These results indicate that the membrane potential change triggered by neuronal activity depends on the cell body location, suggesting that the astrocytic membrane potential is coupled to local neuronal activity.

For hippocampal astrocytes, we analyzed their membrane potential during nontheta and theta states (Fig. 6*A*,*B*), which roughly correspond to the synchronized and desynchronized states of the cortex (Wolansky et al., 2006). The membrane potential of an astrocyte showed slow oscillations during nontheta states, whereas the membrane potential rhythmically oscillated at ~4 Hz with a smaller amplitude during theta activity. During nontheta states, sharp waves were seen in the stratum radiatum LFP, and sharp-wave-associated ripple activity was seen in the stratum pyramidale (Fig. 6*A*). Similar to cortical astrocytes, the mean membrane potential of hippocampal astrocytes was similar in nontheta and theta states (Fig. 6*C*) (-88.3 ± 4.6 vs -86.6 ± 4.2 mV, $p = 0.2$, t test). The membrane potential fluctuation of hippocampal astrocytes during nontheta states was 0.56 ± 0.24 mV ($n = 26$), representing higher values than during the theta state (Fig. 6*D*) (0.31 ± 0.11 mV, $n = 24$, $p < 0.0005$, t test). For

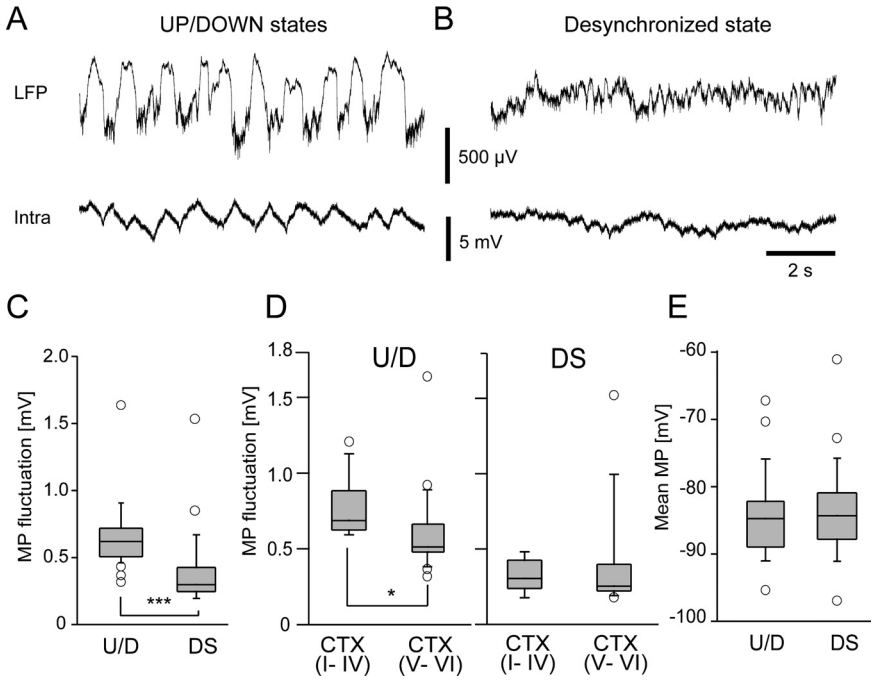

Figure 4. Membrane potential (MP) fluctuations of cortical astrocytes in different LFP states. ***A***, Extracellular LFP (upper trace) and membrane potential fluctuations of a single cortical astrocyte (bottom trace) are plotted during the synchronized state (U/D). ***B***, Similar plots taken from the same cell as in ***A*** during the desynchronized state (DS). ***C***, ***D***, Fluctuation amplitude is significantly larger during the synchronized state (***$p < 0.001$, *t* test) and the upper cortical layer (I–IV) astrocytes elicit larger membrane potential fluctuations during synchronized states (*$p < 0.05$), but they are indistinguishable during the desynchronized state. ***E***, Mean membrane potential was similar in synchronized and desynchronized states.

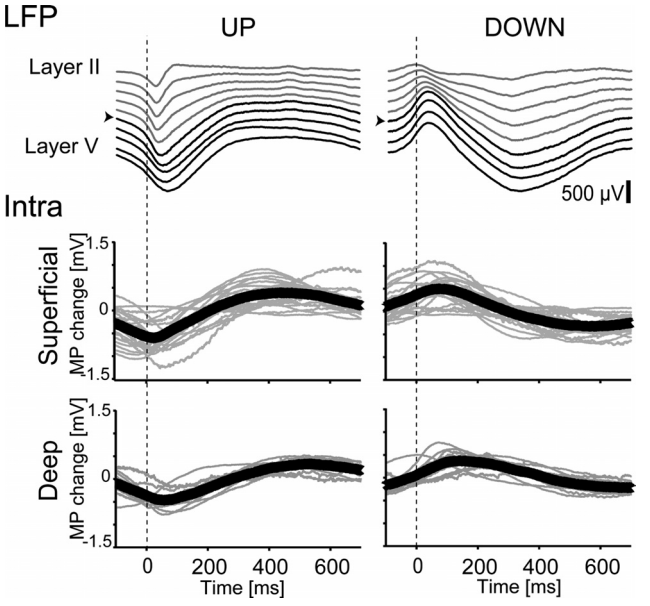

Figure 5. Astrocytic membrane potential (MP) change triggered by UP and DOWN states. Example of triggered averaging of LFP (upper panel) by onset and offset UP states. The traces are from a multichannel silicon probe with linearly arranged recording sites (100 μm apart). Superficial layer traces (layer II–IV) are in gray and deep layer traces (layer V–VI) are in black. The channel indicated by the arrowhead was used to calculate onsets and offsets of UP states for triggered averaging. Population data of the triggered averaging of membrane potential transition of astrocytes with UP and DOWN states (lower panel). Gray lines are triggered averaging of membrane potential transitions of individual astrocytes. The means of the traces are in bold lines.

the cells in which stable recordings were obtained in both LFP states, pairwise *t* test fluctuations during the nontheta state (Fig. 6*E*) ($p < 0.0001$, paired *t* test).

Next we examined the membrane potential change of astrocytes in each layer of the hippocampus during sharp-wave-associated ripple oscillations, as sharp waves represent massively synchronized input from CA3 pyramidal cells (Buzsáki, 1986). Interestingly, triggered averaging of astrocytic membrane potential showed different profiles in each layer (Fig. 6*F*). The astrocytes in stratum pyramidale (Pyr, $n = 3$) reached peak depolarization in 20 ms from trigger point, whereas astrocytes in stratum radiatum (Rad, $n = 9$) and in stratum lacunosum-moleculare (LM, $n = 5$) depolarized significantly slower and reached a peak within 500 ms. In stratum oriens (Ori, $n = 3$), astrocytes showed an intermediate profile. In all layers, the membrane potential decayed over 1 s after the sharp-wave-driven membrane depolarization peak.

Discussion

We recorded membrane potential fluctuations of astrocytes in cerebral cortex and hippocampus of mature (>P28) rats *in vivo*. Intracellular labeling with BDA-10000 and the subsequent immunohistological processing allowed unambiguous identification of the recorded astrocytes (Mishima et al., 2007). We investigated the diversity in astrocytes using a combination of physiological and anatomical techniques. We found that astrocytes are hyperpolarized below −80 mV and the membrane potential fluctuations range within a few millivolts. In agreement with previous reports (Amzica and Steriade, 2000; Amzica and Massimini, 2002; Amzica et al., 2002), the slow membrane potential fluctuations highly correlate with the surrounding neuronal activity. These physiological properties appeared to be common among the recorded astrocytes and did not show obviously segregated subpopulations when the astrocytes were classified by GFAP expression level. The degree of membrane potential fluctuation, however, did show a significant variability according to the cell body location. To our knowledge, this is the first study where *in vivo* behavior of astrocytic membrane potential dynamics in different layers of cortical systems are compared. These findings are discussed further below.

Correlation of astrocyte properties with GFAP expression

GFAP is a member of the cytoskeletal protein family and thought to be important for modulation of astrocyte morphology and motility by providing structural stability to astrocytic processes (Eng et al., 2000). GFAP has been suggested to play an important role in synaptic plasticity, as GFAP-null mice display impaired LTD in the cerebellum (Shibuki et al., 1996) and enhanced LTP in the hippocampus (McCall et al., 1996). Moreover, GFAP expression is regulated by neuronal activity (Steward et al., 1991). Interestingly, several studies have reported the existence of astrocytes with undetectable levels of GFAP. For example, layer III and IV astrocytes are devoid of GFAP(+) cells even though astrocytes are distributed homogeneously among layer II to VI

(Gabbott and Stewart, 1987; Stichel et al., 1991). As there has been a controversy over diversity of astrocytes in the expression of GFAP (Walz and Lang, 1998; Walz, 2000; Ogata and Kosaka, 2002), we questioned whether diversity in GFAP expression has any implications in *in vivo* physiological properties of astrocytes.

We found that ~70% and 80% of the intracellularly labeled astrocytes were GFAP(+) in the cerebral cortex and hippocampus, respectively. Despite the distinct expression levels of GFAP, we saw little difference in the input resistance, mean membrane potential, and membrane potential fluctuation between GFAP(+) and GFAP(−) astrocytes.

A wide range of glial resting membrane potentials have previously been described in *in vitro* preparations (McKhann et al., 1997; D'Ambrosio et al., 1998). In our *in vivo* study, the mean membrane potential of astrocytes had a unimodal distribution with a mode at −86 mV. The heterogeneity in astrocytic resting membrane potentials reported previously could be due to different developmental maturation states (Zhou et al., 2006; Houades et al., 2008). As our recordings were performed in adult rats, it is highly plausible that all of the astrocytes we recorded are "passive astrocytes" that represent mature astrocytes. Indeed, our *in vivo* data suggest mature cortical and hippocampal gray matter astrocytes are less heterogeneous and support the decrease of heterogeneity due to maturation reported in *in vitro* studies (Zhou et al., 2006, 2009; Houades et al., 2008). In addition, we found that the GFAP expression level of an astrocyte bore no relationship with the astrocytic occupancy volume, which is in line with a previous observation by Ogata and Kosaka (2002).

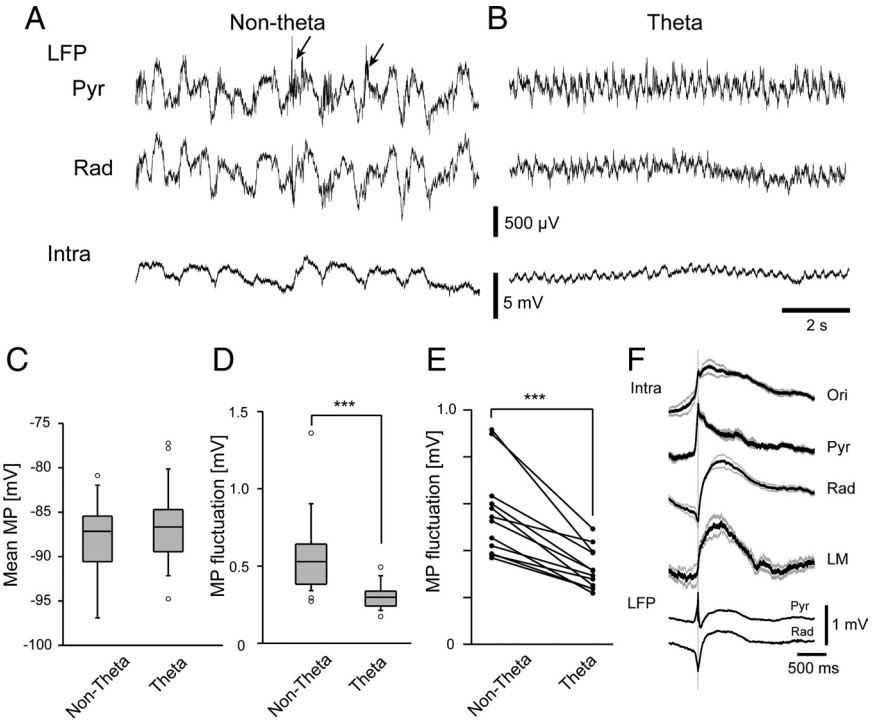

Figure 6. Membrane potential fluctuations of hippocampal astrocytes in different LFP states. ***A***, Extracellular LFPs from the CA1 stratum pyramidale (upper trace), stratum radiatum (middle trace), and the membrane potential of a single hippocampal astrocyte (bottom trace) are plotted during the nontheta state. Arrowheads indicate the occurrences of sharp-wave-associated ripple oscillations. ***B***, Similar plots taken from the same cell (bottom trace) as in ***A*** during the theta state. Pyr, Stratum pyramidale; Rad, stratum radiatum. ***C***, Mean membrane potential was similar in nontheta and theta states ($p = 0.2$, *t* test). ***D***, Membrane potential fluctuation amplitude is significantly larger during nontheta states than theta states (***$p < 0.001$, *t* test). ***E***, Similar decreases of fluctuations at the single cell level are observed in those experiments that allow pairwise comparisons of membrane potential fluctuations from the same cells (***$p < 0.001$, paired *t* test). ***F***, Sharp-wave-triggered averaging of astrocyte membrane potential in different layers of hippocampal CA1 before and after trigger (solid line). Gray lines show ±SEM.

Our present results are somewhat against our initial expectations as distinct physiological diversities have been reported in *in vitro* studies. For instance, based on the existence of functional glutamate transporters and AMPA receptors, GluT and GluR cells have been proposed for GFAP promoter transgenic mice (Matthias et al., 2003; Wallraff et al., 2004; Jabs et al., 2005). Moreover, GluT cells have lower input resistance (~10 MΩ) than GluR cells (~70–270 MΩ), analogous to input resistance differences between GFAP(+) and GFAP(−) glial cells (Seifert and Steinhauser, 1995; Wallraff et al., 2004; Zhou et al., 2006). In our data, we could not uncover any distinct difference in the input resistance by GFAP expression level. Altogether, our results indicate that the GFAP expression level of the mature astrocyte is not reflected in the cell's basic electrophysiological and morphological properties. Since transgenic expression of GFP using a GFAP promoter does not necessarily result in expression of the protein exclusively in astrocytes, the most parsimonious explanation of the GluT and GluR cells is that the former are astrocytes and the latter are NG2 cells.

Membrane potential fluctuation of astrocytes

As gray matter protoplasmic astrocytes have mutually exclusive territories (Bushong et al., 2002; Halassa et al., 2007) and the current flow between astrocytes is small (Xu et al., 2007; Meme et al., 2009), the membrane potential fluctuations of an astrocyte should separately reflect the local neuronal activity. The membrane potential depolarization onset of superficial layer astrocytes preceded that of deeper layer astrocytes in the cortex by ~30 ms. Likewise, the offset of membrane potential depolarization was earlier in superficial layers. The phenomenon can be explained by considering the intracortical connections in the sensory cortex; layer 4 neurons project to layer 2/3, which in turn project to layer 5. LFPs also indicate earlier transition from the UP state to the DOWN state in superficial layers. Therefore, astrocytic membrane potential depolarization has a tight relationship with the LFP.

Which aspect of neuronal activity is involved in astrocytic depolarization? Previously, glutamate transporter and inward K^+ currents have been identified as responsible for astrocytic membrane potential depolarization upon afferent stimulation in the olfactory bulb (De Saint Jan and Westbrook, 2005). Glutamate transporter current has a fast response and the current disappears as extracellular glutamate is taken up (<50 ms). On the other hand, inward K^+ current lasts longer (>100 ms). A large proportion of the K^+ component is due to activity in postsynaptic neurons (De Saint Jan and Westbrook, 2005). Given the slow (subsecond) oscillatory pattern of membrane potential dynamics during synchronized state in the cortex and during sharp-wave-associated ripples in the hippocampus, we attribute this finding to the extracellular potassium concentration ($[K^+]_o$) due to neuronal discharge activity. In fact, in the cat cerebral cortex, $[K^+]_o$

and astrocytic membrane potential depolarization was shown to be tightly correlated *in vivo* (Amzica et al., 2002) in cats. *In vitro* studies reported concomitant extracellular K^+ ($[K^+]_o$) and membrane potential depolarization of astrocytes evoked by electrical stimulation (Ballanyi et al., 1987; Casullo and Krnjevic, 1987; Meeks and Mennerick, 2007). The change of $[K^+]_o$ can be predicted based on a membrane potential versus $[K^+]_o$ curve, in which a slope of 54.8 mV per 10-fold change in $[K^+]_o$ was estimated in hippocampal slice (Meeks and Mennerick, 2007). Assuming a Nernstian relationship with a basal $[K^+]_o$ of 3.5 mM and a resting membrane potential of −86 mV, 1–5 mV of astrocytic membrane potential depolarization observed in our study corresponds to ~0.15–0.82 mM increase of $[K^+]_o$.

In the hippocampus, astrocytes depolarize in synchrony with the occurrences of sharp-wave-associated ripples. To our knowledge, our results are the first description of astrocytic membrane potential transition correlating with spontaneous LFP events in the hippocampus. The time course of the ripple-triggered averaging of membrane potential of astrocyte showed ~1 mV depolarization, and the time course profiles were slightly different in various layers. Similar to the cortex, the time course is slow in the hippocampus. It is notable that the stratum pyramidale, where the largest amplitude of ripple oscillations is recorded, receives GABAergic inputs from local interneurons, whereas glutamatergic inputs from CA3 terminate in stratum oriens and stratum radiatum. Such spatial segregation of synaptic input could contribute to the layer-dependent depolarization profile.

In conclusion, our study suggests a relatively homogeneous astrocyte population in the gray matter of the mature cerebral cortex and hippocampus. The mean membrane potential of astrocytes was hyperpolarized below −80 mV and was similar across different LFP states. Such hyperpolarized membrane potential is potentially desirable to maintain constant amino-acid transporter activity.

References

Amzica F, Massimini M (2002) Glial and neuronal interactions during slow wave and paroxysmal activities in the neocortex. Cereb Cortex 12:1101–1113.

Amzica F, Steriade M (2000) Neuronal and glial membrane potentials during sleep and paroxysmal oscillations in the neocortex. J Neurosci 20:6648–6665.

Amzica F, Massimini M, Manfridi A (2002) Spatial buffering during slow and paroxysmal sleep oscillations in cortical networks of glial cells *in vivo*. J Neurosci 22:1042–1053.

Bakiri Y, Attwell D, Káradóttir R (2009) Electrical signalling properties of oligodendrocyte precursor cells. Neuron Glia Biol 13:1–9.

Ballanyi K, Grafe P, ten Bruggencate G (1987) Ion activities and potassium uptake mechanisms of glial cells in guinea-pig olfactory cortex slices. J Physiol 382:159–174.

Bushong EA, Martone ME, Jones YZ, Ellisman MH (2002) Protoplasmic astrocytes in CA1 stratum radiatum occupy separate anatomical domains. J Neurosci 22:183–192.

Buzsáki G (1986) Hippocampal sharp waves: their origin and significance. Brain Res 398:242–252.

Casullo J, Krnjević K (1987) Glial potentials in hippocampus. Can J Physiol Pharmacol 65:847–855.

D'Ambrosio R, Wenzel J, Schwartzkroin PA, McKhann GM 2nd, Janigro D (1998) Functional specialization and topographic segregation of hippocampal astrocytes. J Neurosci 18:4425–4438.

De Saint Jan D, Westbrook GL (2005) Detecting activity in olfactory bulb glomeruli with astrocyte recording. J Neurosci 25:2917–2924.

Eng LF, Ghirnikar RS, Lee YL (2000) Glial fibrillary acidic protein: GFAP-thirty-one years (1969–2000). Neurochem Res 25:1439–1451.

Gabbott PL, Stewart MG (1987) Distribution of neurons and glia in the visual cortex (area 17) of the adult albino rat: a quantitative description. Neuroscience 21:833–845.

Halassa MM, Fellin T, Takano H, Dong JH, Haydon PG (2007) Synaptic islands defined by the territory of a single astrocyte. J Neurosci 27:6473–6477.

Houades V, Koulakoff A, Ezan P, Seif I, Giaume C (2008) Gap junction-mediated astrocytic networks in the mouse barrel cortex. J Neurosci 28:5207–5217.

Jabs R, Pivneva T, Hüttmann K, Wyczynski A, Nolte C, Kettenmann H, Steinhäuser C (2005) Synaptic transmission onto hippocampal glial cells with hGFAP promoter activity. J Cell Sci 118:3791–3803.

Kuffler SW, Nicholls JG, Orkand RK (1966) Physiological properties of glial cells in the central nervous system of amphibia. J Neurophysiol 29:768–787.

Matthias K, Kirchhoff F, Seifert G, Hüttmann K, Matyash M, Kettenmann H, Steinhäuser C (2003) Segregated expression of AMPA-type glutamate receptors and glutamate transporters defines distinct astrocyte populations in the mouse hippocampus. J Neurosci 23:1750–1758.

McCall MA, Gregg RG, Behringer RR, Brenner M, Delaney CL, Galbreath EJ, Zhang CL, Pearce RA, Chiu SY, Messing A (1996) Targeted deletion in astrocyte intermediate filament (Gfap) alters neuronal physiology. Proc Natl Acad Sci U S A 93:6361–6366.

McKhann GM 2nd, D'Ambrosio R, Janigro D (1997) Heterogeneity of astrocyte resting membrane potentials and intercellular coupling revealed by whole-cell and gramicidin-perforated patch recordings from cultured neocortical and hippocampal slice astrocytes. J Neurosci 17:6850–6863.

Meeks JP, Mennerick S (2007) Astrocyte membrane responses and potassium accumulation during neuronal activity. Hippocampus 17:1100–1108.

Meme W, Vandecasteele M, Giaume C, Venance L (2009) Electrical coupling between hippocampal astrocytes in rat brain slices. Neurosci Res 63:236–243.

Mishima T, Sakatani S, Hirase H (2007) Intracellular labeling of single cortical astrocytes in vivo. J Neurosci Methods 166:32–40.

Nedergaard M, Ransom B, Goldman SA (2003) New roles for astrocytes: redefining the functional architecture of the brain. Trends Neurosci 26:523–530.

Nishiyama A, Yang Z, Butt A (2005) Astrocytes and NG2-glia: what's in a name? J Anat 207:687–693.

Nolte C, Matyash M, Pivneva T, Schipke CG, Ohlemeyer C, Hanisch UK, Kirchhoff F, Kettenmann H (2001) GFAP promoter-controlled EGFP-expressing transgenic mice: a tool to visualize astrocytes and astrogliosis in living brain tissue. Glia 33:72–86.

Ogata K, Kosaka T (2002) Structural and quantitative analysis of astrocytes in the mouse hippocampus. Neuroscience 113:221–233.

Picker S, Pieper CF, Goldring S (1981) Glial membrane potentials and their relationship to [K+]o in man and guinea pig. A comparative study of intracellularly marked normal, reactive, and neoplastic glia. J Neurosurg 55:347–363.

Sakatani S, Seto-Ohshima A, Itohara S, Hirase H (2007) Impact of S100B on local field potential patterns in anesthetized and kainic acid-induced seizure conditions in vivo. Eur J Neurosci 25:1144–1154.

Schipke CG, Haas B, Kettenmann H (2008) Astrocytes discriminate and selectively respond to the activity of a subpopulation of neurons within the barrel cortex. Cereb Cortex 18:2450–2459.

Seifert G, Steinhäuser C (1995) Glial cells in the mouse hippocampus express AMPA receptors with an intermediate Ca2+ permeability. Eur J Neurosci 7:1872–1881.

Seigneur J, Kroeger D, Nita DA, Amzica F (2006) Cholinergic action on cortical glial cells in vivo. Cereb Cortex 16:655–668.

Shibuki K, Gomi H, Chen L, Bao S, Kim JJ, Wakatsuki H, Fujisaki T, Fujimoto K, Katoh A, Ikeda T, Chen C, Thompson RF, Itohara S (1996) Deficient cerebellar long-term depression, impaired eyeblink conditioning, and normal motor coordination in GFAP mutant mice. Neuron 16:587–599.

Steward O, Torre ER, Tomasulo R, Lothman E (1991) Neuronal activity up-regulates astroglial gene expression. Proc Natl Acad Sci U S A 88:6819–6823.

Stichel CC, Müller CM, Zilles K (1991) Distribution of glial fibrillary acidic protein and vimentin immunoreactivity during rat visual cortex development. J Neurocytol 20:97–108.

Sugimori M, Preston RJ, Kitai ST (1978) Response properties and electrical constants of caudate nucleus neurons in the cat. J Neurophysiol 41:1662–1675.

Takata N, Hirase H (2008) Cortical layer 1 and layer 2/3 astrocytes exhibit distinct calcium dynamics in vivo. PLoS ONE 3:e2525.

Wallraff A, Odermatt B, Willecke K, Steinhäuser C (2004) Distinct types of astroglial cells in the hippocampus differ in gap junction coupling. Glia 48:36–43.

Wallraff A, Köhling R, Heinemann U, Theis M, Willecke K, Steinhäuser C (2006) The impact of astrocytic gap junctional coupling on potassium buffering in the hippocampus. J Neurosci 26:5438–5447.

Walz W (2000) Controversy surrounding the existence of discrete functional classes of astrocytes in adult gray matter. Glia 31:95–103.

Walz W, Lang MK (1998) Immunocytochemical evidence for a distinct GFAP-negative subpopulation of astrocytes in the adult rat hippocampus. Neurosci Lett 257:127–130.

Wang X, Lou N, Xu Q, Tian GF, Peng WG, Han X, Kang J, Takano T, Nedergaard M (2006) Astrocytic Ca2+ signaling evoked by sensory stimulation in vivo. Nat Neurosci 9:816–823.

Wolansky T, Clement EA, Peters SR, Palczak MA, Dickson CT (2006) Hippocampal slow oscillation: a novel EEG state and its coordination with ongoing neocortical activity. J Neurosci 26:6213–6229.

Xu HT, Pan F, Yang G, Gan WB (2007) Choice of cranial window type for in vivo imaging affects dendritic spine turnover in the cortex. Nat Neurosci 10:549–551.

Zhou M, Kimelberg HK (2000) Freshly isolated astrocytes from rat hippocampus show two distinct current patterns and different [K(+)](o) uptake capabilities. J Neurophysiol 84:2746–2757.

Zhou M, Kimelberg HK (2001) Freshly isolated hippocampal CA1 astrocytes comprise two populations differing in glutamate transporter and AMPA receptor expression. J Neurosci 21:7901–7908.

Zhou M, Schools GP, Kimelberg HK (2006) Development of GLAST(+) astrocytes and NG2(+) glia in rat hippocampus CA1: mature astrocytes are electrophysiologically passive. J Neurophysiol 95:134–143.

Zhou M, Xu G, Xie M, Zhang X, Schools GP, Ma L, Kimelberg HK, Chen H (2009) TWIK-1 and TREK-1 are potassium channels contributing significantly to astrocyte passive conductance in rat hippocampal slices. J Neurosci 29:8551–8564.